Proceedings of the 2002 IEEE
International Conference on Robotics & Automation
Washington, DC • May 2002

Modeling of Needle Insertion Forces for Robot-Assisted Percutaneous Therapy

C. Simone and A. M. Okamura
Department of Mechanical Engineering
Engineering Research Center for Computer Integrated Surgical Systems and Technology
The Johns Hopkins University, Baltimore, MD 21218
csimone@titan.me.jhu.edu, aokamura@jhu.edu

Abstract

Force information from needle insertions was measured and modeled for use in robot-assisted percutaneous therapies. Data was collected on bovine livers using the Johns Hopkins University Steady Hand Robot, and modeled in three parts: force due to capsule stiffness, friction, and cutting. Capsule stiffness is modeled by a nonlinear spring model, friction by a modified Karnopp model, and cutting by the remaining forces, which appear to be constant for a given tissue sample. During robot-assisted procedures, real-time force data can be compared to these models to control puncture of interior structures. Future work will combine imaging with force data to characterize tissue layers in specific applications, such as liver ablation and prostate brachytherapy.

1. Introduction

Percutaneous therapies are diagnostic or therapy delivery procedures that involve the insertion of tubular delivery devices into targeted locations in the body with the aid of intra-operative imaging devices (e.g., CT, MRI, ultrasound, and fluoroscopy). These delivery apparatuses include instruments such as needles, trocars, bone drills, screws, laser devices, etc. While minimally invasive surgery reduces patient discomfort and decreases recovery time, a major shortcoming is reduced visual and tactile information transmitted to the physician via the instruments. Current clinical methods involve an iterative manual technique of imaging and positioning, which lacks real-time presentation of information to the operator.

We focus on the needle as the delivery instrument. For many needle insertions, it is vital that the physician have detailed control of the needle position and velocity, since the area surrounding the target location can often be easily damaged. Complicating factors include tissue deformation before puncture, needle bending, relaxation of the tissue after puncture, and reduced tactile and visual information. These procedures require rapid reaction time and control greater than typical human ability. However, there exist some cues that can assist the physician. The amount of force necessary to pierce and travel through different layers of tissue varies based on the material (skin, muscle, fluid, ligament, etc.). Forces also change with needle depth and angle of insertion.

The use of cooperative robotic systems for positioning and manipulating therapy delivery devices presents the option of simultaneous human and computer control. While the physician cannot directly feel interaction forces, information can be transmitted through the robot. In addition, the surgeon can request that the robot apply virtual fixtures to assist or guide in task execution. The primary goal of this work is to develop haptic models of percutaneous therapies that can be used to provide appropriate robotic assistance.

Reality-based models, which are developed from measurements of actual tissues, can be used for automatic monitoring of progress and event detection in both freehand and robot-assisted procedures. Instrumented tools or cooperative robots can enhance the human ability to recognize events during needle insertion by providing additional visual, aural, or haptic feedback. The work discussed in this paper will demonstrate reality-based models that can provide real-time haptic feedback with cooperative surgical robots, thereby greatly improving

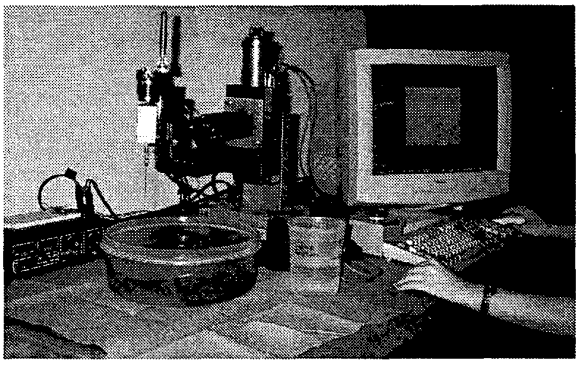

Figure 1. The data acquisition system was comprised of the JHU Steady Hand Robot, a needle holder with load cell, and a control computer.

accuracy, consistency, therapy delivery speed, and reduction of patient discomfort.

1.1 Previous Work

To date, a number of researchers have explored ways to improve surgeons' skills in procedures where little visual and direct tactile feedback exists. These mainly take the form of haptic simulators for catheter insertion [7], lumbar puncture [8], epidural blocks [2] [11], endoscopic surgeries [17], laparoscopic surgeries [14], and prostate biopsies [3]. While most of the previous work has focused on improving clinical therapies through training, our goal is to develop models that can be used in real-time robotic assistance.

In the areas of telemanipulation and human-robot cooperation, there are a few examples of reality-based modeling used in medical procedures. Yen, *et al.* [18] describe a telemanipulation system for assisting in the penetration of soft tissue for medical tasks. The system interacts with the environment through a rotating arm that performs needle insertion. They construct a simulation using velocity and acceleration information calculated from encoder readings of a single test of a porcine sample. Brett, *et al.* [1] present an automated handheld drill to interpret the type and deformation of tissue while drilling through the stapes bone of the ear. Components measured include syringe pressure, force, and needle displacement. The instrument's movements are not restricted but rely solely on the surgeon for direction. There has also been recent work in the area of surgical devices to acquire *in vivo* data [4,13].

The cooperative manipulation system we use in this work is the Johns Hopkins University Steady Hand Robot. This surgical assistance system allows for interactive cooperation between machines and physicians, augmenting human capabilities to achieve manipulation with the precision and sensitivity of a machine, but the manipulative transparency and accessibility of hand-held instruments [16]. Minimally invasive procedures involve conditions of significant sensitivity, which especially benefit from such systems. In order to effectively use the assistive capabilities of the SHR, real time data must be compared with models and appropriate, contextual assistance provided.

2. Data Acquisition

Data was acquired using the JHU Steady Hand Robot as a 1-degree-of-freedom motion device to guide a 1.27mm O.D., 15.24cm long surgical needle with a beveled tip into bovine liver. A 1-axis 10N capacity Entran™ load cell was used to measure forces in the direction of motion. The control software executed on a Windows NT Pentium II 450 MHz computer with a graphical user interface that we developed. We recorded time, position of the needle, and force at a frequency of

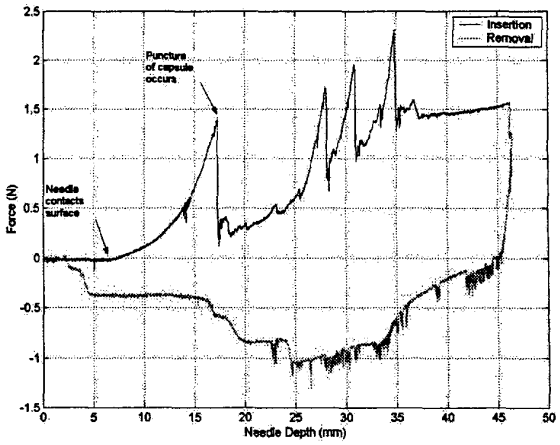

Figure 2. Typical force vs. position plot showing insertion and removal forces, and events such as puncture.

500 Hz. Data was acquired from three bovine livers (one cow and two steers). Figure 1 shows the robot acquiring data on one of the samples.

3. Property Estimation

In order to accurately model the haptic needle insertion experience, it is necessary to separate the data into its components. To the best of the authors' knowledge, there has been no prior work regarding the separation of force into components for the purposes of modeling. Graphs of the data (Figure 2) reveal two main phases: pre-puncture and post-puncture. The main puncture event is designated by a peak in force after a steady rise, followed by a sharp decrease. Subsequent variations in force are due to friction, cutting forces, and internal stiffness, as well as collisions with, and puncture of interior structures. The force data collected is a summation of stiffness, friction, and cutting forces, as shown in Equation 1. The stiffness force is pre-puncture, and the friction and cutting forces post-puncture. We consider cutting forces to include the plastic deformation from cutting as well as the force resulting from tissue stiffness at the tip of the needle.

$$f_{needle}(x) = f_{stiffness}(x) + f_{friction}(x) + f_{cutting}(x) \quad (1)$$

Before we proceed, it is necessary to note the anatomy of the liver. Because this organ functions to filter and process blood, it contains a substantial number of arteries and veins. The structural and functional units of the liver are ~2mm, hexagonally-shaped lobules which are comprised of liver cells arranged in one-cell-thick plate-like layers that radiate from the central vein to the edge of the lobule (Figure 3). At each of the six corners of a lobule is a portal triad, consisting of a branch of the hepatic artery, hepatic portal vein, and a bile duct [12]. It is for this reason that several puncture events (identified

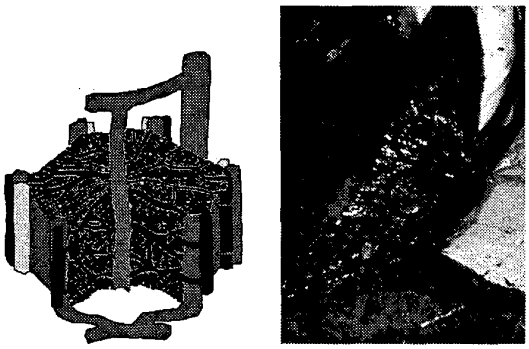

Figure 3. Three-dimensional representation of one liver lobule, which includes many interior structures, (left, adapted from [12]), and a cutaway of one of the livers used in the experiments, revealing large interior vessels (right).

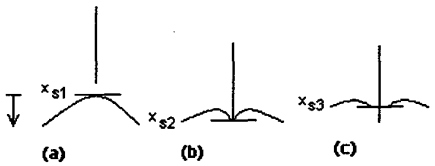

Figure 4. Locations of the tissue surface at different stages of needle insertion. (a) pre-puncture (b) puncture (c) post-puncture.

by elevated forces and subsequent sudden drops in force) are noted after the initial penetration in Figure 2.

3.1 Stiffness

The stiffness force is due to the elastic properties of the organ and its capsule. The elasticity of the tissue can be identified from pre-puncture forces in the insertion data. We performed numerous insertions at a constant velocity of 3 mm/s within a 10 cm^2 area on bovine livers 1 and 2. The general form of the force on the needle is described by the relationship

$$f_{stiffness} = \begin{cases} 0 & x_{tip} < x_{s1} \\ f(x) & x_{s1} \le x_{tip} \le x_{s2} \\ 0 & x_{tip} > x_{s3} \end{cases}, \qquad (2)$$

where $f(x)$ is a one-dimensional quasi-static stiffness model, and x_{tip} and x_{s1}, x_{s2}, x_{s3} are the positions of the needle tip and tissue surface relative to a fixed coordinate system before puncture. The relative locations of x_{s1}, x_{s2}, and x_{s3} can be seen in Figure 4. All positions are considered to be relative to a fixed coordinate system. The position x_{s3} is less than x_{s2} due to relaxation of the tissue after puncture.

Biological tissue is linearly elastic for small deformations [6]. However, it is clear from our data that

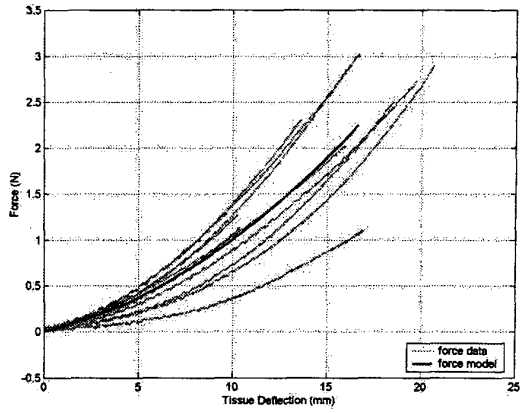

Figure 5. Typical stiffness data for a bovine liver before membrane puncture within a 10 cm^2 area.

there is a large amount of deformation before puncture, so the force must be modeled using a nonlinear method. In the search for a relation to model the deformation of the tissue, we first attempted to use a nonlinear spring model as demonstrated by d'Aulignac *et al.* [5] in modeling deformation of a human thigh. That relation is given by

$$f(x) = \frac{x}{ax+b}, \qquad (3)$$

where x is the difference in the length of the springs with respect to their original, resting length. The parameters a and b were fitted to match the deformation measured on bovine livers. However, lower rms error values were found using a second order polynomial of the form

$$f(x) = a_1 x + a_2 x^2, \qquad (4)$$

which best fits the experimental data. In our model, we make the assumption that the force is zero before the needle contacts the surface, so we set the intercept to zero. The coefficient values are presented in Table 1. The values corresponding to the second liver match the data better due to the difference in area over which the data were recorded for the two livers (with r^2 values of 0.98 for liver #2 as compared to 0.88 for liver #1). Different locations in the liver are likely to have variations in stiffness values due to the presence of internal structures as noted in Figure 3. Insertions performed on the second

Table 1. Values of the nonlinear stiffness parameters (a_0, a_1, a_2) for modeling samples.

Liver #	a_1 [N/m]	a_2 [N/m^2]
1	0.0480	0.0052
2	0.0020	0.0023

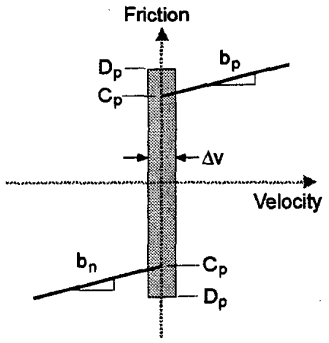

Figure 6. Modified Karnopp friction model (adapted from [15]).

liver were distributed over a much smaller area, resulting in more consistent stiffness measurements. Because this model may not be appropriate under viscoelastic conditions, more complete biomechanical models are currently under consideration, such as those put forth by Fung [6].

Without the use of an imaging system, forces and needle positions must be used to determine when puncture occurs. Based on 19 measurements of needle insertions on a liver with the capsule intact, the maximum force before puncture averaged 2.3040 ± 0.8286 N, occurring at a needle depth of 16.6514 ± 3.5470 mm (corresponding to x_{s2} in Figure 4) after coming in contact with the tissue surface. This maximum force is followed by a sudden drop in force to an average of 0.6579 ± 0.5638 N.

3.2 Friction

The friction force occurs along the length of the needle, and is due to tissue adhesion and damping. For this reason, a modified Karnopp friction model is considered (Figure 6). This representation accounts for the "stiction" phenomenon by having the static value of friction higher than the dynamic value. The model equation is

$$F_{friction}(\dot{x},F_a)=\begin{cases} C_n\,\mathrm{sgn}(\dot{x})+b_n\dot{x} & \dot{x}\le -\Delta v/2 \\ \max(D_n,F_a) & -\Delta v/2<\dot{x}\le 0 \\ \min(D_p,F_a) & 0<\dot{x}<\Delta v/2 \\ C_p\,\mathrm{sgn}(\dot{x})+b_p\dot{x} & \dot{x}\ge \Delta v/2 \end{cases} \quad (4)$$

where C_n and C_p are the negative and positive values of dynamic friction, b_n and b_p are the negative and positive damping coefficients, D_n and D_p are the negative and positive values of static friction, $\dot{x}$ is the relative velocity between the needle and tissue, $\Delta v/2$ is the value below which the velocity is considered to be zero, and F_a is the sum of non-frictional forces applied to the system.

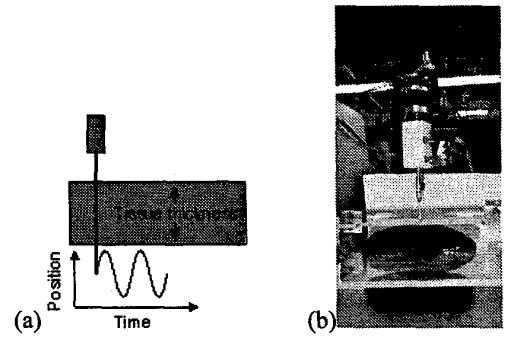

Figure 7. Sinusoidal motion of the needle during friction experiments. (a) Graphical representation (b) Experimental setup.

In order to properly identify the friction and damping coefficients, we used periodic force data obtained by passing a needle completely through one lobe of a liver whose thickness is known so that there is always a constant amount of tissue in contact with the needle at any given time (Figure 7). To limit pre-sliding displacement of the liver and maintain a constant thickness of tissue while the needle is in motion, an adjustable-height platform was designed and constructed with holes in order to allow the needle to pass completely through a lobe of the liver while constraining the deflection of the tissue as the needle inserts and withdraws. The liver thickness was recorded for each insertion. The robot was programmed to move the needle at frequencies of 0.2, 0.5, and 0.8 Hz for 7-10 cycles. Repeated sinusoidal motion along the same vertical line prevents cutting of new tissue, resulting in force measurements due to friction and inertia alone. Three data sets for each frequency were taken at different locations in a 258 gram liver piece.

The data was analyzed using modified Matlab™ code provided by Richard [15]. Velocity and force data, along with a fit of the friction model, is shown in Figure 8. The average positive damping value, b_p per unit length of needle in tissue, was 904 Ns/m^2, and the average negative damping value, b_n per unit length of needle in tissue, was 458 Ns/m^2. The values of the damping coefficients varied widely for the different frequencies (we recorded a maximum 1327 Ns/m^2 of at 0.2 Hz and a minimum of 377 Ns/m^2 at 0.8 Hz), indicating that a more complex model is warranted if differing needle insertion speeds are to be used. The average positive and negative coefficients of dynamic friction (C_p and C_n) were zero (to within the noise of the force data). This is due to the lubricating blood contained within the liver. The average positive and negative coefficients of static friction (D_p and D_n) per unit length of needle in tissue were 30.4 and –29.3 N/m, respectively.

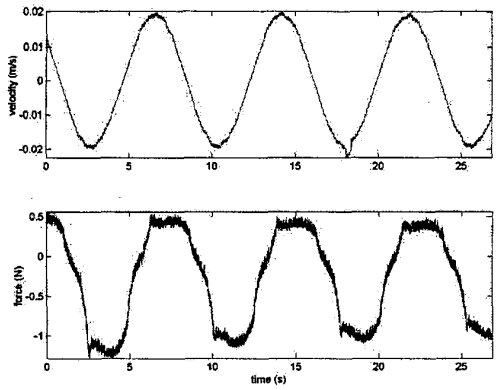

(a)

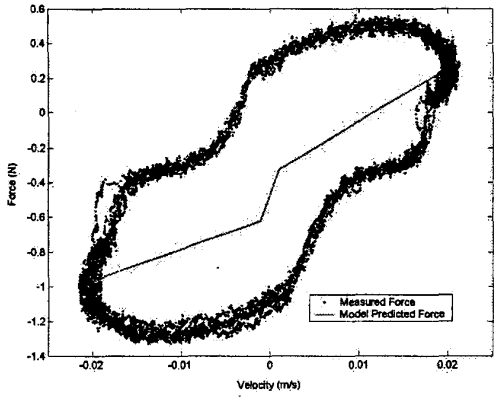

(b)

Figure 8. Friction data for sinusoidal motion of the needle through a 3.1 cm thick liver sample at 0.2 Hz. The top plot (a) shows velocity and force versus time. The bottom plot (b) shows force vs. velocity for the original data and the Karnopp friction model.

The plates used in these experiments were intended to prevent significant pre-sliding displacement, by constraining the pull of the tissue in the direction opposite to that of needle motion. One negative aspect of this method is that the liver is slightly compressed between the plates and only a segment of the organ is tested. However, we performed several preliminary constant velocity insertions without these constraints and observed that the force measurements were comparable. Nevertheless, some pre-sliding displacement occurred, resulting in the hysteresis apparent in Figure 8b. Current experiments involve the use of an imaging system (fluoro/CT) to measure the relative velocities of the tissue and needle, allowing us to remove the constraints and in the future use a bristle or Dahl friction model [10]. A model that includes pre-sliding displacement will likely give more consistent results, as tissue deformation clearly occurs prior to relative motion between the needle and tissue.

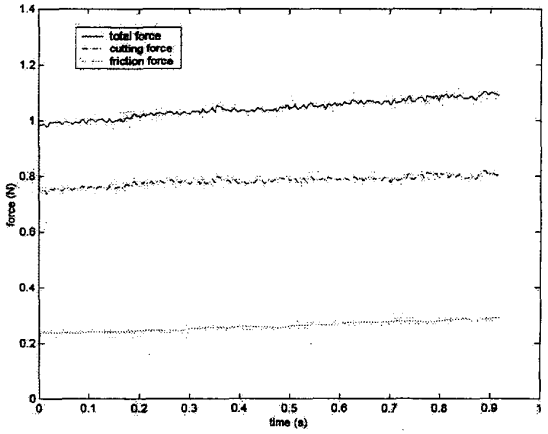

Figure 9. Forces on the needle tip during insertion at 3 mm/s. The total force is separated into its cutting force and friction force components.

3.3 Cutting

The cutting force is that which is necessary to slice through the tissue. We postulate that this force exists as a combination of cutting forces and tissue stiffness at the tip of the needle, since the needle still encounters stiffness as it cuts through new tissue. The cutting force is isolated by subtracting the previously determined friction force from the total force. Ideally, cutting forces will be constant, and therefore unrelated to needle depth. The relation for cutting force is given by

$$f_{cutting} = \begin{cases} 0 & x_{tip} \le x_{s2}, t < t_p \\ f_{cutting} & x_{tip} > x_{s3}, t \ge t_p \end{cases}, \qquad (3)$$

where $f_{cutting}$ is a constant for a given tissue, x_{tip} and x_{s2}, x_{s3} are the position of the needle tip and tissue surface relative to a fixed coordinate system before puncture, t is time, and t_p is the time of puncture. Equation 3 assumes that the depth of the needle tip in the tissue monotonically increases with time.

For five needle insertions into a liver at 3 mm/s, the average cutting force was 0.94 ± 0.36 N. The cutting force was calculated by subtracting the friction force from the total force. The friction force was determined by

$$f_{frcition} = b_p l v_{needle}, \qquad (4)$$

where b_p is the damping coefficient per unit length (we chose b_p = 1327 Ns/m^2, which corresponds to a slow insertion speed), l is the length of the needle in the tissue, and v_{needle} is the velocity of the needle tip. The primary difficulty in determining cutting forces was finding insertion data segments free of collisions with internal vessels. (The presence of these vessels is evidenced by Figures 2 and 3). These internal collisions add an

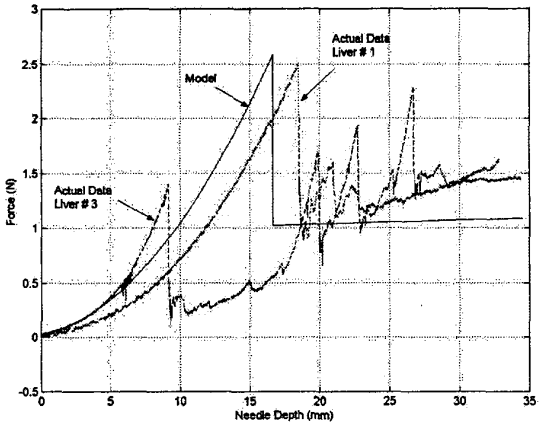

Figure 10. The needle insertion model is compared to two insertions on real livers. Although the general shape is similar, the model cannot exactly match the data because of the wide variation in insertion forces and collisions with unmodeled internal structures.

additional stiffness force that should not be taken into account when measuring the cutting force of the liver tissue. Because of this factor, the measured cutting forces were not quite constant, but increased slightly with insertion depth. An example of cutting forces, separated from the stiffness and friction data, is shown in Figure 9.

4. Model Application and Future Work

Use of the model developed in the previous sections necessitates validation by comparison with additional needle insertions, the assembly of a tissue library describing the model parameters, and automatic event detection for application in robot-assisted procedures.

4.1 Model Validation

The model is validated by direct comparison of simulated and real data. Based on the average parameter values obtained in the previous section, a complete model of the needle insertion experience has been created. The model, as well as data from real needle insertions, can be compared in Figure 10. The overall shape of the model is similar to the data, although the significant variations in the data from one liver to the next make a perfect match nearly impossible. One problem is that collisions with small interior structures such a blood vessels are not included in the model. These add additional peaks and stiffness forces to the data. We also make the assumption that the needle remains completely straight as it travels through the tissue, while in reality there are small deflections. It is relevant to note that other needle parameters exist, such as velocity, tip type, and diameter. Despite these limitations of the model, it may be still be used for event detection and haptic simulations.

4.2 Tissue Library

Model parameters can be determined and stored in a "tissue library," which is based on the elastic, friction, and plastic (cutting) properties of the desired target and tissues in the vicinity of the organ (such as blood vessels). These models can then be used for simulation and as a basis for real-time comparison during robot-assisted procedures for automatic event detection. Much like the "Visible Human," a "Haptic Human" could be used by surgeons for both planning and training. One limitation in developing an accurate model is the difficultly of obtaining *in vivo* data. Some data exists on various tissues, but traditional solid materials testing methods were used as opposed to measurements involving instrument-tissue interactions [9]. The solution is to design biologically compatible instrumented surgical tools that can log data during use in regular procedures, such as those developed in [4,13].

4.3 Application in Robot-Assisted Procedures

There are numerous ways in which these models can be used in robot-assisted procedures. The needle could be made to stop at a specified location, or stop upon an event such as puncture. In addition, the needle could be automatically withdrawn slightly to account for tissue relaxation after puncture. Knowledge of the peak force through tissue may be used to limit velocity and guide the needle before puncture. Once it is known that the needle has entered the desired organ, it may use the real-time force measurements to detect undesired collision and accordingly stop the motion.

After further research, it will be possible to maintain relative zero motion of a needle with respect to the tissue by ensuring that the forces remain at a certain level, accounting for motion of organs due to breathing. Another goal is to develop models for insertion into many different tissues, and use the models to differentiate between materials as the needle passes through. In order to test our current model's applicability in robot-assisted procedures, we are currently developing an assistive experiment. In real time, the model and data will be compared to detect the initial puncture of a liver and the movement of the needle tip into a tissue other than liver (simulated in this case by air as a "control tissue," to eliminate unknown friction and cutting forces).

5. Conclusions

Automatic compensation for variations in deformation and forces that arise during needle insertion is a worthwhile concept to implement into computer integrated surgical systems. Autonomous and robot-assisted procedures can compare real-time forces against stored models in order to detect and identify events, thereby responding immediately and appropriately.

In this work, we demonstrated the development of models and their utility in comparisons with real-time force data. Our approach identified the three main force components: stiffness, friction, and cutting, enabling us to accurately identify events in a needle insertion procedure. Benefits of a complete system include improved event detection and reaction time, guidance of velocity and position, and increased accuracy and reliability. Applications include various image-guided percutaneous therapies, such as liver ablation and prostate brachytherapy.

Additional research will be necessary to make the data models more complete. Further experiments are being conducted in combination with an imaging system (fluoro/CT) for more accurate measurement of the relative motion between the needle and tissue. We also plan to incorporate an accelerometer to obtain vibration measurements for event detection. Improved biomechanical models taking into account tissue viscoelasticity [6] and pre-sliding displacement will also be considered. The advent of devices to obtain *in vivo* data modeling will also play a role in developing better models. The final models will be integrated into assistive procedures, autonomous procedures, and haptic virtual environments. Eventually, once these haptic techniques are perfected, it may even be possible to limit the amount of intra-operative imaging in percutaneous procedures, thereby providing the added benefit of minimizing X-ray exposure to operating room staff and patients.

Acknowledgements

The authors wish to acknowledge the support of the National Science Foundation under the Engineering Research Center grant #EEC9731478. Friction modeling software was provided by Dr. C. Richard. Dr. R. Kumar, Dr. A. Bzostek, A. Morris, Dr. D. Burschka and Dr. G. Fichtinger are thanked for their assistance and advice.

References

[1] P.N. Brett, A.J. Harrison, and T.A. Thomas, "Schemes for the Identification of Tissue Types and Boundaries at the Tool Point for Surgical Needles," *IEEE Trans. Information Technology in Biomedicine*, Vol. 4, No. 1, 2000, pp. 30-36.

[2] P. N. Brett, et al., "Simulation of resistance forces acting on surgical needles," *Proceedings of the Institution of Mechanical Engineers, Part H*, Vol. 211 (H4), 1997, pp. 335-347.

[3] P. N. Brett and R. S. W. Stone, "A technique for measuring contact force distribution in minimally invasive surgical procedures," *Proceedings of the Institution of Mechanical Engineers, Part H*, Vol. 211 (H4), 1997, pp. 309-316.

[4] I. Brouwer, et al., "Measuring In Vivo Animal Soft Tissue Properties for Haptic Modeling in Surgical Simulation," *Medicine Meets Virtual Reality 2001*, pp. 69-74.

[5] D. d'Aulignac, R. Balaniuk, and C. Laugier, "A Haptic Interface for a Virtual Exam of the Human Thigh," *Proceedings of the 2000 IEEE International Conference on Robotics & Automation*, pp. 2452-2456.

[6] Y.C. Fung, Biomechanics: Mechanical Properties of Living Tissues, 2nd ed., New York: Springer-Verlag, 1993, pp. 277.

[7] E. Gobbetti, et al., "Catheter Insertion Simulation with Co-registered Direct Volume Rendering and Haptic Feedback," *Medicine Meets Virtual Reality 2000*, pp. 96-98.

[8] P. Gorman, et al., "A Prototype Haptic Lumbar Puncture Simulator," *Proceedings of Medicine Meets Virtual Reality 2000*, pp. 106-109.

[9] K. Hayashi, H. Abé, and M. Sato, Data Book on Mechanical Properties of Living Cells, Tissues, and Organs, New York: Springer, 1996.

[10] V. Hayward and B. Armstrong, "A new computational model of friction applied to haptic rendering," Experimental Robotics VI, P. Corke and J. Trevelyan, Eds., Lecture Notes in Control and Information Sciences, Vol. 250, Springer-Verlag, 2000, pp. 403-412.

[11] L. Hiemenz, et al., "A Physiologically Valid Simulator for Training Residents to Perform an Epidural Block," *Proc. 1996 IEEE Biomedical Engineering Conference,* pp. 170-173.

[12] E.N. Marieb, Human Anatomy & Physiology, 5th ed., Menlo Park, CA: Benjamin/Cummings, 1997, pp. 920-921.

[13] M.P. Ottensmeyer and J.K. Salisbury, Jr., "*In Vivo* Data Acquisition Instrument for Solid Organ Mechanical Property Measurement," *Medical Image Computing and Computer-Assisted Intervention 2001*, pp. 975-982.

[14] S. Payandeh, "Force Propagation Models in Laparoscopic Tools and Trainers," *Proc. 1997 IEEE Engineering in Medicine & Biology International Conference*, pp. 957-960.

[15] C. Richard, M. R. Cutkosky, and K. MacLean, "Friction Identification for Haptic Display," *Proceedings of the American Society of Mechanical Engineers, Dynamic Systems and Control Division*, Vol. 67, pp. 327-334.

[16] R. Taylor, et al., "Steady-Hand Robotic System for Microsurgical Augmentation," *The International Journal of Robotics Research*, Vol. 18, No. 12, 1999, pp. 1201-1210.

[17] V. Vuskovic, et al., "Realistic Force Feedback for Virtual Reality Based Diagnostic Surgery Simulators," *Proc. 2000 IEEE International Conference on Robotics & Automation*, pp. 1592-1598.

[18] P. Yen, R. D. Hibberd, B. L. Davies, "A Telemanipulator System As An Assistant And Training Tool For Penetrating Soft Tissue," *Mechatronics*, Vol. 6, No. 4, 1996, 423-436.